
White Rose Research Online

eprints@whiterose.ac.uk
https://eprints.whiterose.ac.uk
Universities of Leeds, Sheffield and York

Deposited via The University of York.

White Rose Research Online URL for this paper:
https://eprints.whiterose.ac.uk/id/eprint/200205/

Preprint:
Clivati, Cecilia, Meda, Alice, Donadello, Simone et al. (2020) Coherent phase transfer for real-world twin-field quantum key distribution. [Preprint]

Reuse
Items deposited in White Rose Research Online are protected by copyright, with all rights reserved unless indicated otherwise. They may be downloaded and/or printed for private study, or other acts as permitted by national copyright laws. The publisher or other rights holders may allow further reproduction and re-use of the full text version. This is indicated by the licence information on the White Rose Research Online record for the item.

Takedown
If you consider content in White Rose Research Online to be in breach of UK law, please notify us by emailing eprints@whiterose.ac.uk including the URL of the record and the reason for the withdrawal request.



arXiv:2012.15199v1 [quant-ph] 30 Dec 2020

Coherent phase transfer for real-world twin-field quantum key distribution

Cecilia Clivati[1,*], Alice Meda[1,2], Simone Donadello[1], Salvatore Virzì[1,3], Marco Genovese[1], Filippo Levi[1], Alberto Mura[1], Mirko Pittaluga[4,5], Zhiliang L. Yuan[4], Andrew J. Shields[4], Marco Lucamarini[6], Ivo Pietro Degiovanni[1,2], and Davide Calonico[1]

[1]INRIM, strada delle cacce 91, 10134 Torino, Italy
[2]INFN, sezione di Torino, via P. Giuria 1, 10125 Torino, Italy
[3]Physics Department, University of Torino, via P. Giuria 1, 10125 Torino, Italy
[4]Toshiba Europe Ltd, 208 Science Park, Milton Rd, Cambridge CB40GZ, U.K.
[5]School of Electronic and Electrical Engineering, University of Leeds, Leeds LS2 9JT, U.K.
[6]Department of Physics and York Centre for Quantum Technologies, University of York, YO10 5DD York, U.K.
[*]c.clivati@inrim.it

January 1, 2021

Abstract

Quantum mechanics allows the distribution of intrinsically secure encryption keys by optical means. Twin-field quantum key distribution is the most promising technique for its implementation on long-distance fibers, but requires stabilizing the optical length of the communication channels between parties. In proof-of-principle experiments based on spooled fibers, this was achieved by interleaving the quantum communication with periodical adjustment frames. In this approach, longer duty cycles for the key streaming come at the cost of a looser control of channel length, and a successful key-transfer using this technique in a real world remains a significant challenge. Using interferometry techniques derived from frequency metrology, we developed a solution for the simultaneous key streaming and channel length control, and demonstrate it on a 206 km field-deployed fiber with 65 dB loss. Our technique reduces the quantum-bit-error-rate contributed by channel length variations to <1%, representing an effective solution for real-world quantum communications.

Quantum key distribution (QKD) enables to share secret cryptographic keys between distant parties, whose intrinsic security is guaranteed by the laws of quantum mechanics [1–3]. Besides pioneering experiments involving satellite transmission [4, 5], the challenge is now to integrate this technology on the long-distance fiber networks already used for telecommunications [6–15]. The maximum secure key rate for QKD decreases exponentially with the channel losses. Although the reach could be extended using quantum repeaters, the related research is still at a rudimentary level and these devices are far from operational [16–18]. Nowadays, intercity distances could only be covered using trusted nodes [13], whose security represents however a significant technical issue. A fundamental resource for next-generation long-distance secure communications is represented by the recently proposed twin-field QKD (TF-QKD) protocol [19], because of its weaker dependence on channel loss.

In TF-QKD, the information is encoded as discrete phase states on dim laser pulses generated at distant Alice and Bob terminals and sent through optical fiber to a central node, Charlie, where they interfere. This idea, sketched in Fig. 1a, was proved secure against general attacks [20–24] also in the finite-size scenario [25–27] and with the aid of two-way communication [28], but it is based on the critical assumptions that the optical pulses are phase-coherent in Alice and Bob and preserve coherence throughout the path to Charlie. While the first requirement can be fulfilled by phase-locking the two QKD lasers in Alice and Bob to a common reference laser transmitted through a service channel, the uncorrelated fluctuations of the length and refractive index of the connecting paths (i.e. the optical length) introduce phase noise to the system and reduce the visibility of the interference measurement. In proof-of-principle experiments

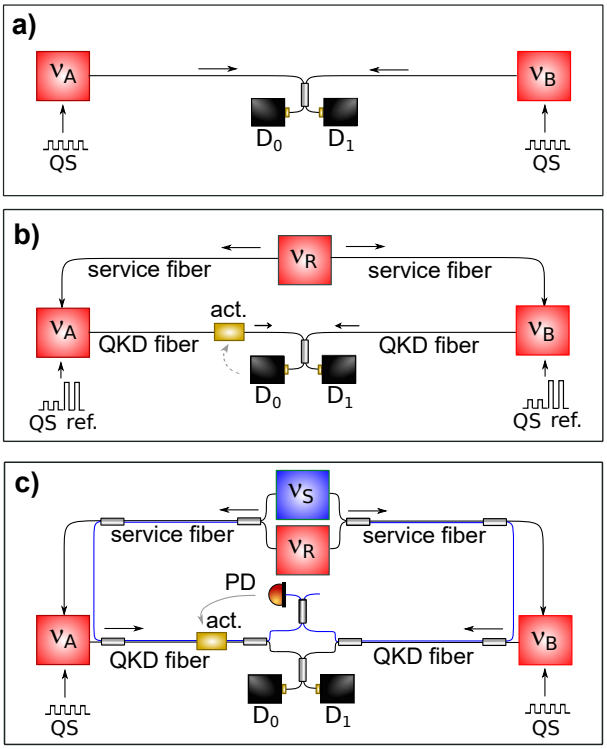

Figure 1: **Principle schemes of TF-QKD.** a) In ideal TF-QKD, Alice and Bob encode quantum states (QS) on local lasers, attenuated to the single-photon level and with equal frequencies $\nu_A = \nu_B$. The resulting signals are sent to Charlie, where they interfere on single-photon detectors (D_0 and D_1). b) In practical implementations, a reference laser with frequency ν_R is sent to Alice and Bob through a service fiber, to phase-lock the QKD lasers and ensure $\nu_A = \nu_B = \nu_R$. After information encoding, QKD lasers are sent to Charlie through the QKD fibers, whose optical-length-changes are detected by interleaving the key streaming with classical transmission. Optical length fluctuations are counteracted by adjusting the phase of the lasers through an actuator (act.). c) In our approach, an additional sensing laser, with frequency ν_S travels the service fiber with the reference laser, and the QKD fibers together with the QKD lasers. It can be spectrally separated because ν_S falls in a different channel of the wavelength-division-multiplexing grid. While QKD lasers interfere on D_0 and D_1, the classical signals at ν_S are phase-compared on a photodiode (PD) to detect the noise of both the service and QKD fibers. This allows tight control of the fiber noise and simultaneous key streaming.

based on spooled fibers [29–33], this effect was mitigated by interleaving the QKD frames with classical transmission frames that were used to periodically realign the phases of interfering pulses [29, 30] (see Fig. 2b). However, this approach becomes less effective as the length of connecting paths exceeds few hundreds of kilometers [29, 32, 33] and there is no experimental evidence that it could work in deployed fibers, where the attenuation and phase fluctuations are considerably higher [34].

We propose a solution derived from frequency metrology. In this context, the transmission of coherent laser radiation over thousand-kilometer-long fibers is employed to compare distant atomic clocks at the highest accuracy [35–41]. This is made possible by the use of ultrastable lasers and the active cancellation of the noise introduced by connecting fibers [42], and the same approach can be exploited in TF-QKD. We realised an apparatus suitable for TF-QKD where the phase fluctuations of both the lasers and connecting fibers are actively cancelled. This is achieved by transmitting an additional laser in the same fiber as the QKD lasers in a wavelength-multiplexed approach. In Charlie, this is used to sense and stabilize the channels' optical length variations (see Fig. 1c). In a QKD experiment, this allows simultaneous key streaming and channels stabilization, ensuring longer duty-cycles and a tighter control of the optical phase on long-haul deployed fibers, where interleaved approaches would fail. We implement our solution on a real-world network where the distance between Alice and Bob is 206 km and the net losses are as high as 65 dB, demonstrating a significant progress over existing quantum communication field trials [6–15], all limited to <100 km distance and <25 dB channel loss.

The experiment

Experimental setup

The map and detailed scheme of our experiment are shown in Fig. 2. We use a pair of ultrastable lasers with a linewidth of ∼1 Hz and frequency ν_R =194.4 THz (1542.14 nm) and ν_S =194.25 THz (1543.33 nm), which are standard frequencies of the dense wavelength-division multiplexed (DWDM) grid. The former (hereafter, reference laser) is used as a reference for locking the QKD lasers in Alice and Bob terminals, and is frequency stabilized to a high-finesse ultrastable Fabry-Perot cavity [43]. The latter (hereafter, sensing laser) is used to detect the fiber noise and allows its cancellation. In our experiment, we offset-locked it to the reference laser using an optical frequency comb [44], although alternative techniques are possible (see Methods). They are combined using a commercial 100 GHz-wide DWDM filter and sent to Alice and Bob through separate service fibers.

At the remote terminals, the reference laser is extracted and used to phase-lock the local QKD laser. This is recombined with the sensing laser and sent back to Charlie on the QKD fiber. This setup implements what is needed for transmitting quantum information, nonetheless we do not realise a fully-operative QKD transmission since this is a technical issue already demonstrated elsewhere [29–32]. Instead, our experiment focuses on improving the system coherence, which is the essential prerequisite for any TF-QKD protocol.

In Charlie, we interfered the QKD lasers in classical and photon-counting regimes, the latter after attenuating the QKD lasers to the single-photon level. As the sensing laser travels the path from Charlie to Alice and Bob together with the reference laser on the service fiber, and the backward path together with the QKD laser on the QKD fiber, its accumulated phase contains information on the optical length changes of connecting paths, that can be used to stabilize them. The incoming beams at the two wavelengths are routed to separate detectors: photons from the QKD lasers interfere on a photodiode (when doing experiments in the classical regime) or a single-photon detector (SPD, in the photon counting regime), while the sensing laser beams are indirectly phase-compared using a pair of photodiodes and a radio-frequency mixer. From it, the relative changes in the optical paths are extracted and stabilised by a phase-locked loop. This is achieved by adjusting the phase of the sensing laser as it travels the acusto-optic modulator AOMa, on Alice's branch. Because the QKD laser also travels through the actuator, its optical phase is stabilised as well (see Methods).

We implemented this scheme over long-haul fiber backbones connecting INRIM, in the city of Torino (Italy), where the Charlie terminal was located, to network nodes separated by 114 km and 92 km of optical fiber with 35 dB and 30 dB losses (Alice and Bob terminals respectively). The overall length of the fiber connecting Alice and Bob was thus 206 km with an attenuation as high as 65 dB. The average loss coefficient of 0.3 dB/km is higher than the specified level for standard optical fibers (0.2 dB/km) and includes discrete losses of the connectors and DWDM equipment, which play a significant role in deployed networks. These fibers are part of the Italian Quantum Backbone and carry other services, among which is the dissemination of atomic clock signals to research facilities of the Country [35, 36]. While conventional fiber communication protocols are based on data exchange over fiber pairs, in which each fiber allows light propagation in a single direction, we implemented a bidirectional transmission on a single fiber, using different DWDM channels for opposite directions. Using this approach, the second fiber of the pair was dedicated to the sensing and QKD lasers only (see Methods). The service fibers carry, in addition to the reference and sensing lasers, also standard data traffic and time/frequency information, which can be conveniently used to implement ultra-precise modulation of the quantum signals and transmit the classical information typical of any QKD protocol, including TF-QKD. Here, we used a White Rabbit precise time protocol [45, 46] to distribute clock information for the optical phase-lock of the QKD laser in Bob.

Results

Fig. 3 shows the interference between the QKD lasers measured on a photodiode in Charlie in a 2 ms time frame, without (a, blue) and with (b, red) active stabilization of the fiber paths. In an unstabilized condition, several phase cycles are accumulated in the considered interval, with an instantaneous drift of up to 30 rad/ms. When the path is stabilized, on the contrary, the phase remains stable over the whole acquisition frame. In this measurement, the phase was stabilized on purpose at a point where its fluctuations were directly mapped into intensity fluctuations, which enabled us to compute the corresponding phase noise power spectral density. This is shown in Fig. 3c: in an unstabilized condition (blue) the phase noise rapidly diverges at low Fourier frequencies, while, when stabilization is activated

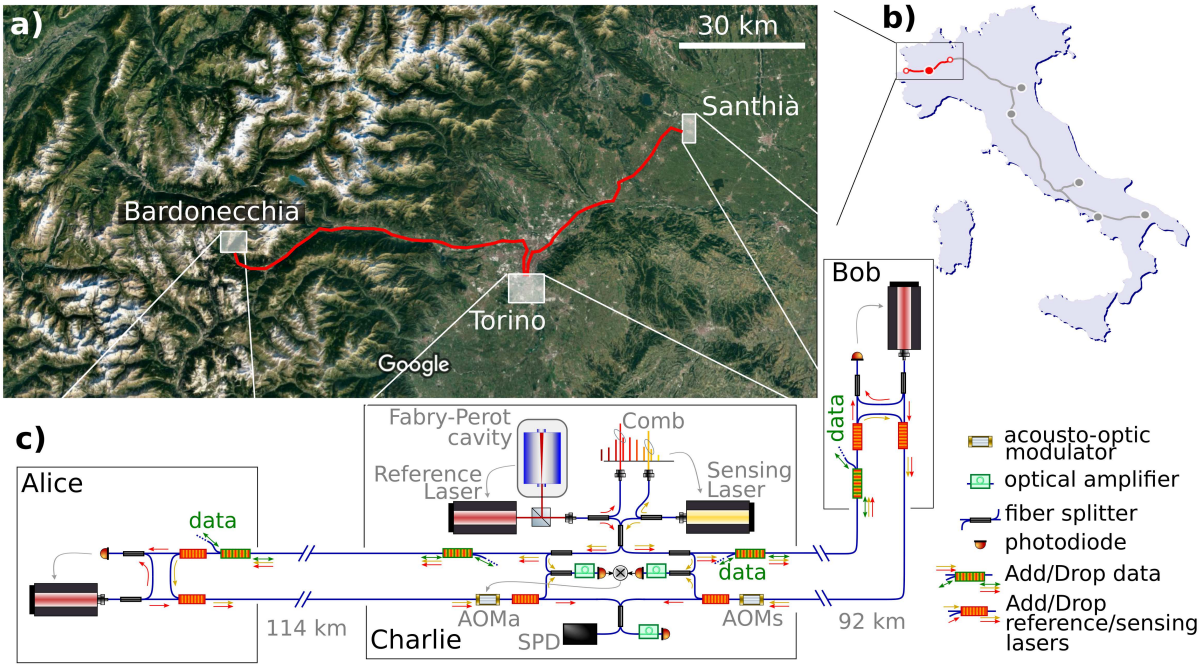

Figure 2: **Map and experimental set-up.** a) Charlie was located at INRIM (Torino), while Alice and Bob were located in shelters of the telecom network in Bardonecchia and Santhià (Imagery ©2020 Landsat/Copernicus, Imagery ©2020 TerraMetrics, Map data ©2020). b) A sketch of the Italian Quantum Backbone, with the spans used in this experiment coloured in red and the red-filled (empty) circles representing Charlie (Alice and Bob). c) The experimental layout. The reference laser in Charlie is stabilized to a high-finesse cavity and the sensing laser is phase-locked to it using an optical comb. Wavelength division multiplexers combine/separate them and add/drop bidirectional data signals. In Alice and Bob, we detect the beat between the incoming reference laser and a local laser and phase-lock the two. The QKD laser light is recombined with the sensing laser and sent to Charlie on a dedicated fiber. The acousto-optic modulator AOMa adjusts the optical phase to correct for the noise introduced by the fiber optical length variations, while AOMs is a fixed frequency shifter. The fiber noise is detected by interfering the local sensing laser with return light from each arm. The two beatnotes are detected on separate photodiodes and phase-compared in the RF domain. The QKD lasers interfere on a photodiode when performing experiments in the classical regime, and on a single photon detector (SPD) in the photon-counting regime, also used to detect background photons.

(red), the noise is suppressed up to a bandwidth of tens of kilohertz. In both traces, the noise floor is set by the QKD lasers at and within the locking bandwidth of 0.9 MHz and the self-delayed interference of the reference and sensing lasers. These contributions are common to the two traces. The latter becomes proportionally higher as the length unbalance between the arms of the interferometer increases and less stable lasers are used. The use of ultrastable lasers was crucial in our setup, where the unbalance was 22 km, i.e. 44 km of differential path considering both the service and QKD fibers. As the relevant noise processes extend up to ∼1 MHz Fourier frequency, we note that an acquisition system with a minimum measurement bandwidth of 2 MHz is required to fully capture them. Devices with slower frequency response would act as low-pass filters, leading to underestimation of the corresponding phase changes.

The QBER associated to phase-decoherence can be calculated from the standard deviation of the phase σ_φ as a function of the frame duration (see Methods). Figure 4 shows the results in a stabilized (red) and unstabilized condition (blue). In both cases, the noise processes responsible for phase fluctuations extinguish at timescales shorter than the inverse of the locking bandwidth of the QKD lasers (indicated by the arrow), making σ_φ negligible. However, in an unstabilized condition, the system exceeds the 1% QBER threshold in about 100 µs. At timescales longer than a few milliseconds, apparently, the phase fluctuations do not increase further. This is an artifact caused by the limited range of the interferometer response, which wraps the phase into the $[0; \pi]$ interval. In practice, the phase wanders by tens of radians in few milliseconds. When stabilization is activated, instead, the system settles in a condition where σ_φ = 0.13 rad, which corresponds to a QBER of 0.5%, for about 100 ms. This value is determined by the residual contribution of the reference, sensing and QKD lasers noise. For a frame duration longer than 100 ms, σ_φ increases due to a non perfect cancellation of the fiber optical length variations. This depends on the fact that such variations are detected through the accumulated phase of the sensing laser, while the reference and QKD lasers accumulate a slightly different phase because of the wavelength difference and uncommon optical paths. This effect is largely predictable and could be reduced with dedicated electronics and an optimised design of the experimental setup, thus allowing further extension of the coherence-time.

The observed residual phase noise and QBER represent conservative estimates, as our measurements were performed on a testbed with as much as 22 km of unbalance between the two arms and with standard telecom diode lasers at the Alice and Bob terminals. Further improvement could be gained using less noisy telecom lasers [47, 48] and faster control techniques. However, already in the present condition, the system can be operated at a QBER $< 3\%$ for timescales of the order of 1 s. Figure 5 shows the interference pattern on a 4 s timescale, and a zoom of a 1 s-long period where the system could be operated at the maximum visibility in a QKD experiment. We also show a zoom of a 100 ms-long region where the interferometer operates far from the deterministic condition. With such a stability, in a QKD experiment, it becomes possible to gather enough photon statistic for realigning the phase on the basis of the QBER, thus virtually ensuring even longer duty cycles.

The same measurements were repeated by attenuating the QKD lasers at the remote terminals by ∼80 dB, so that only few thousands of photons/s reach the detector in Charlie, under similar operating conditions as in recent TF-QKD experiments [29–32]. For this measurement, we replaced the photodiode with an SPD and recorded the number of counts as a function of time. We were able to reproduce the same visibility as with the classical beams, showing substantial agreement between the two approaches.

In view of the implementation of this technique in a QKD experiment, an aspect of concern is the control of the background photons which couple to the QKD fibers from the surrounding environment, or are originated in the QKD fibers themselves due to nonlinear effects. Only photons at the QKD lasers wavelength are relevant to the count, as those in other bands can be filtered out. To counteract the drop in performances of standard DWDM filters outside the C-band, we combined them with broader filters featuring 50 dB attenuation throughout the visible and near infrared spectrum (see Methods). This ensures efficient separation of the sensing and QKD lasers photons, and provides adequate immunity to background photons from external sources even when the network occupancy and its spectral distribution are unknown.

Background photons in the same band as the quantum signal are mainly produced by the Raman scattering of the sensing laser in the QKD fiber. This problem is well known in the context of real-world QKD and forces to use either dedicated fibers or QKD transmission in the O-band at 1310 nm, where the scattering from channels in the C-band is negligible [9, 49]. In our experiment, we could minimise its impact by ensuring that the sensing laser power coupled to the QKD fiber at the Alice and Bob terminals was <1 µW. Another effect contributing photons in the same band as QKD lasers is the Rayleigh scattering of the reference laser happening in the service fiber. Rayleigh-scattered photons propagating backward into the service fiber may fall into the QKD fiber due to evanescent coupling. In our case, the

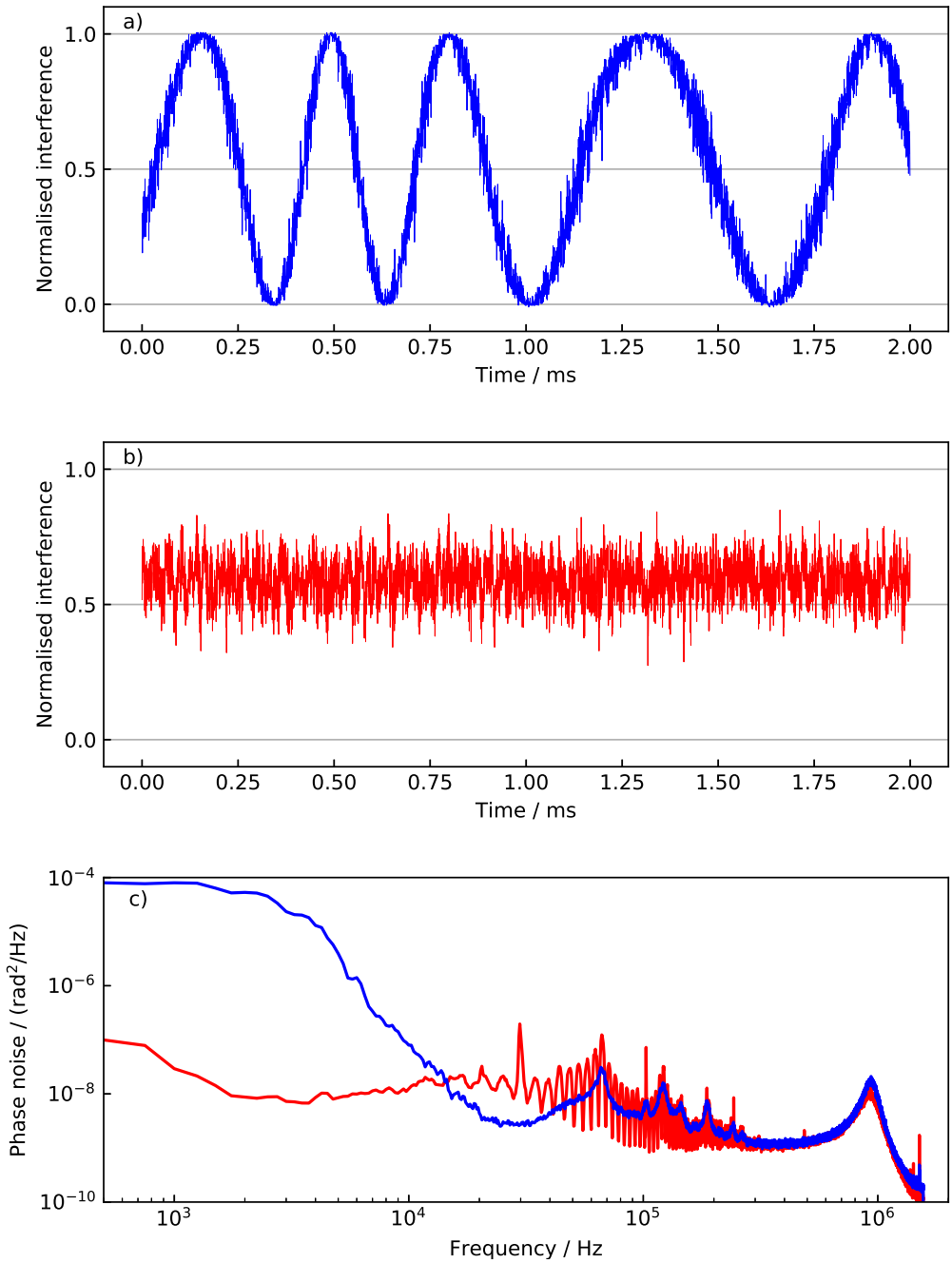

Figure 3: **QKD lasers interference with unstabilized and stabilized fibers**. We record the interference between the QKD lasers in Charlie on a fast photodiode (the traces are normalised between 0 and 1. a) In an unstabilized condition the instantaneous phase drifts by 30 rad/ms and is folded back when it exceeds the $[0 : \pi]$ interval. b) When the fiber is stabilized, the phase remains stable. In this measurement, the interferometer was stabilized far from the folding point, i.e. in a condition where phase fluctuations were directly mapped into intensity fluctuations, to investigate the residual noise processes. c) The power spectral density of the phase. A significant reduction in the noise is observed in a stabilized condition (red) with respect to an unstabilized condition (blue). The apparent plateau observed at low Fourier frequencies in an unstabilized condition is originated by the folding of the interferometer response. At high Fourier frequency, similar noise is observed in the two traces, mainly due to the QKD lasers and the self-delayed interference of the reference and sensing lasers.

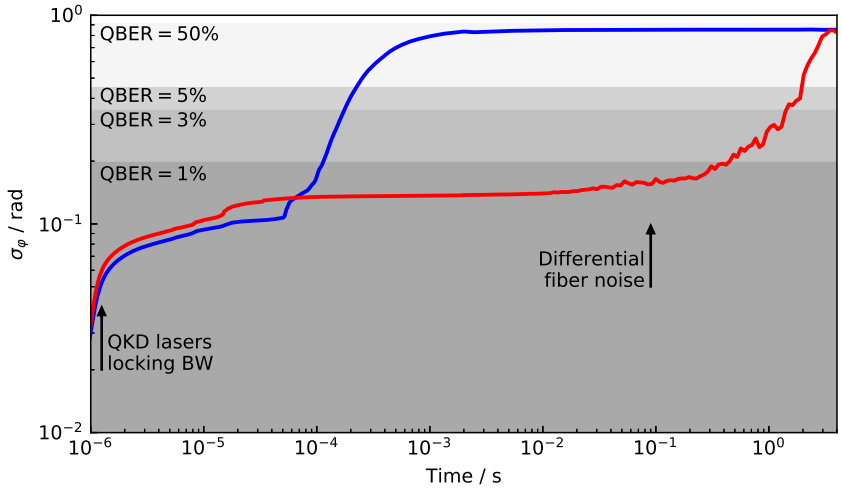

Figure 4: **Phase fluctuations over time.** The deviation of the phase σ_φ between the two QKD lasers interfering in Charlie at different timescales, in an unstabilized (blue) and stabilized (red) condition. For this calculation, we acquired the interference pattern over 4 s and subdivided it in shorter time frames, calculating σ_φ for each frame. The shadowed areas indicate upper thresholds for relevant values of the QBER, quantified as $\sigma_\varphi^2/4$ in the low-noise ($\varphi \approx 0$) approximation. The arrows indicate timescales where the QKD lasers noise and the uncompensated fiber noise (uncorrelated fluctuations at the two wavelengths) become relevant. The phase, and corresponding QBER, were retrieved from the interference pattern according to the procedures described in the Methods.

maximum allowed power for the reference laser was 20 µW, which was still enough for ensuring a stable phase lock of the slave lasers at Alice and Bob terminals. Because this effect is stronger in the first $\sim$ 20 km from Charlie, in case of longer distances or more lossy fibers, Rayleigh scattering could be kept negligible by maintaining the same level of launched power, and exploiting optical amplification closer to remote Alice and Bob terminals.
We measured the background photon rate in our setup exploiting a low noise InGaAs/InP avalanche photodiode with quantum efficiency of 10% and dead time of 25 µs. In the working conditions the observed rate of background photons was $(5.09 \pm 0.01)\,\mathrm{s}^{-1}$, evaluated over 24 h of measurement, primarily attributed to Raman scattering of the sensing laser. When all the laser sources involved in our experiment were switched off, the measured level of background photons was $(4.76 \pm 0.04)\,\mathrm{s}^{-1}$, slightly above the intrinsic dark count rate of our SPD, i.e. $(4.52 \pm 0.03)\,\mathrm{s}^{-1}$, meaning that background photons coupled from nearby fibers or from the metropolitan environment is minimal. Overall, the background photon rate introduced by our apparatus is of the same order of the dark count rate of our SPD, and is expected not to significantly affect the QBER.

Discussion

We realised a setup suitable for TF-QKD and characterised it over a 206 km-long deployed fiber with 65 dB of optical loss. This is the first design for a TF-QKD setup on a commercial network under normal operating conditions and with these losses. This required solution of several fresh challenges for the real-world implementation of TF-QKD, such as a considerably higher attenuation than on spooled fiber (0.3 dB/km on our setup), autonomous and remote-controlled operation of the equipment at the Alice and Bob terminals, which was deployed in telecom shelters in a non-controlled environment, and a considerable unbalance (22 km) in the interferometer arms. Even under these conditions, we ensured the phase coherence of interfering lasers over hundreds of milliseconds, i.e. 1000 times more than what reported so far in laboratory trials. Furthermore, besides temperature, acoustic and seismic noise on the fibers, our scheme also compensates non-stationary events such as those due to antropic activities, and is expected to be robust against further up-scaling of the infrastructure in terms of length, attenuation and phase noise.

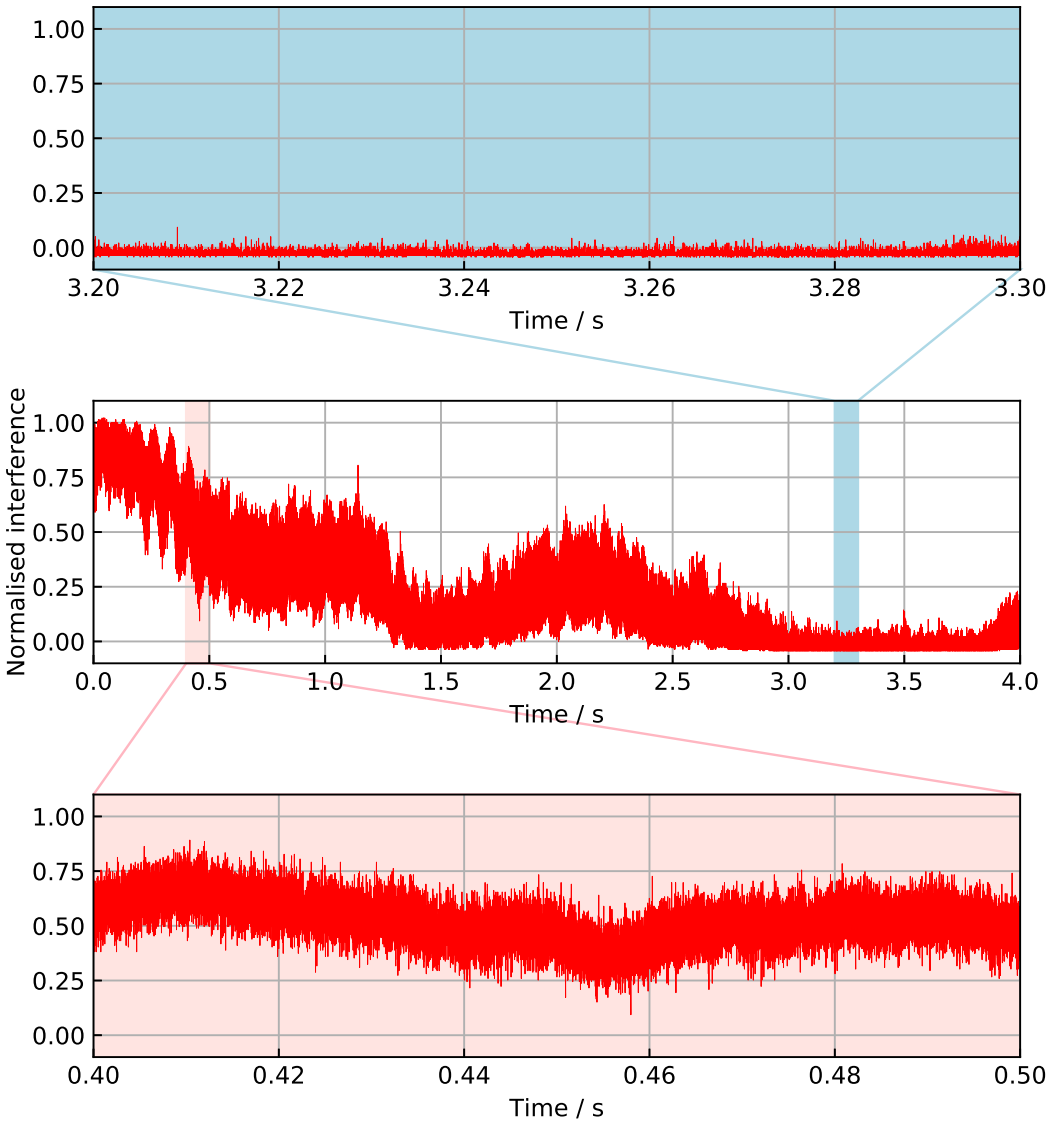

Figure 5: **QKD lasers interference on the long term.** In the central panel, the normalised interference pattern in the stabilized-fiber condition is shown in a 4 s-long time window. The blue shadowed area in the uppermost panel indicates a 100 ms-long fraction of the time interval in which the interferometer operated in the maximum visibility condition, i.e. the one exploited for the exchange of the bits of the cryptographic key. The red shadowed area in the lowermost panel indicates a 100 ms-long time interval in which the interferometer operated around the 0.5 visibility. Configurations far from the deterministic behavior of the interfermeter (i.e. far from the maximum and minimum of the visibility) are the ones where the relation between the phase fluctuations and the QBER is linear, and could be used to realign the phase on the long term and mitigate the residual uncontrolled optical path length variations.

The key points of our technique lie in the use of ultrastable lasers with several hundreds of kilometers of coherence-length, which is mandatory considering the constraints set by the network topology which prevents from realizing perfectly-balanced interferometers, and the simultaneous transmission of separate signals for the fiber noise detection and the key streaming. On one hand, this enables to keep the QBER to manageable levels thanks to a tighter control of the phase; on the other hand, it allows more advantageous duty cycles for the quantum communication. In our experiment we were able to maintain $\sigma_\varphi = 0.13\,\mathrm{rad}$, corresponding to a QBER of 0.5%, for about 100 ms. Both aspects concur to increase the effective key rate, which is a major advantage especially on long haul networks, where rather low rates of a few kb/s must be already taken into account due to the fiber losses [29].
We note that the realised scheme allows rejection of the service fiber noise as well. While previous implementations focus on the strategies for mitigating the noise on the QKD fiber, the issue of noise on the service fiber was only marginally addressed so far [32, 50], proposing the Doppler noise cancellation [42] as an effective solution. However, we note that this approach is bandwidth-limited by the time needed by the light to travel the fiber, and would leave several radians of uncompensated phase fluctuations in a realistic case [42]. In our multiplexed scheme, on the contrary, the noise detection is performed upon recombination in Charlie, and the correction can be applied without delay, thus ensuring a higher suppression. Another approach exploits a Sagnac-interferometer-based configuration [31]. We note that these schemes would suffer from the same limitations as the Doppler stabilization [51]. On the basis of the results obtained in this work, we also foresee the Rayleigh effect as a major source of background photons in a Sagnac loop. Rayleigh scattering poses a limitation on the maximum distance achievable when time division multiplexing strategy is employed [32], while the wavelength division multiplexing strategy we are proposing is free from this limitation.
The proposed scheme can be directly implemented in real quantum communication systems. We underline that, together with phase fluctuation, there are other non-ideal behaviors in the encoding pattern (modulation and phase) of the QKD lasers at the remote terminals that may increase the QBER (i.e. reduction of the visibility interference). Among these, are the relative jitter of the clocks referencing the patterns in Alice and Bob, and the pulses' arrival time in Charlie which is in principle affected by the varying delay added by the fibers. In this perspective, we note that our scheme supports a common clock signal to be delivered to the terminals trough the service fiber. The additional timing delay introduced by the QKD fibers is <1 ps. Thus, provided that the modulation patterns are initially matched to account for the different lengths of the interferometer arms, the fibers delay is not expected to affect the visibility of the interference even at the high modulation rate of $\sim$1 GHz. However, the multiplexed approach used to stabilize the optical phase could be further exploited to compensate for the overall jitter of the service and QKD fibers. Finally, we note that the results of this work are not related to any specific system architecture, and describe useful strategies for a variety of QKD protocols, significantly contributing to the route towards quantum secure communications in a real field.

Acknowledgements

We thank Consortium Top-IX, especially Matteo Frittelli and Alessandro Galardini, for technical assistance on deployed fibers and helpful discussions on the network design; PPQSense for the fruitful collaboration in customizing the lasers drivers.
M.L. has carried out part of this work at Toshiba Europe Ltd.
We acknowledge funding from projects Nato G5263; EMPIR-18SIB06-TIFOON, which has received funding from the EMPIR programme co-financed by the EMPIR Participating States and from the European Union's Horizon 2020 research and innovation programme; OpenQKD (Grant Agreement No 857156) and QCall (675662), both of which were also funded by the EU's Horizon 2020 research and innovation programme.

Author contributions

M.L. and I.P.D. had the initial idea for the work.
C. C., S. D., A. Mu., D. C. designed and developed the experimental setup and performed the measurements in the classical regime.
A. Me., S. V., I. P. D. contributed QKD expertise and performed the measurements in photon-counting regime.
F. L. and M. G. provided fundamental knowledge and insight on key metrological and QKD aspects of

the work and substantially contributed to the experimental design.
M. L., M. P., Z. L. Y., A. J. S. contributed background in TF-QKD and to the design of the experimental setup.
I. P. D., D. C. coordinated the project and supported the experimental activity.
All authors discussed the experimental data and contributed to the analysis of results.
C. C., with contribution from all authors, wrote the paper.

Methods

The optical fiber network

The fibers used for this experiment are part of the Italian quantum backbone, which provides atomic clock dissemination services to scientific and commercial users of the Country [35]. These services, as well as standard data traffic for the remote control of the equipment at the network nodes, require bidirectional optical transmission. To ensure compatibility with QKD, we migrated the traffic to the single service fiber, using different wavelengths for the two directions of propagation. In particular, time/frequency dissemination services used channel 30 and 31 of the International Telecommunication Union (ITU) grid, corresponding to a wavelength of 1553.33 nm and 1552.52 nm respectively. Remote control was established over channels 28 and 29 (wavelengths 1554.94 nm and 1554.13 nm). Standard DWDM multiplexers were used to combine and separate channels 28-31 at the network nodes, while the sensing and reference lasers travelled through the unfiltered ports, which brought ∼2 dB additional losses each.

Reference and sensing lasers

The reference laser is a fiber laser at 1542.14 nm (channel 44 of the 100 GHz-DWDM grid), frequency stabilized to an ultrastable Fabry-Perot cavity with a Finesse of 120'000 using the Pound-Drever-Hall technique [43]. The resulting linewidth is 1 Hz and the short-term instability is 2×10^{-15}. The cavity is made of ultra-low expansion glass, housed in high vacuum and placed on a platform for passive seismic noise damping. We used an external acousto-optic modulator (AOM) as a fast actuator to lock the fiber laser to the cavity. The achieved bandwidth of 200 kHz is limited by the internal delay of the AOM and by its driver. Although diode lasers offer much higher control bandwidths, their phase noise is higher as well, which deteriorates the phase coherence and makes the use of fiber laser preferable for this application. The reference laser is a diode laser at 1543.33 nm. This wavelength lies in the middle between the channels 42 and 43 of the 100 GHz-DWDM grid, and is a standard of the advanced 50 GHz-DWDM grid. We virtually phase-locked it to the reference laser using an optical comb as a spectral bridge. The comb is an octave-spanning Er:fiber femtosecond frequency comb with 250 MHz repetition rate whose spectral emission is centered around 1560 nm. Following the technique described in [44], we detected the beatnote of both lasers with the comb and measured their phase-difference on a mixer. This enabled us to detect the relative phase between the two, which could not be directly measured because of the large spectral separation. The phase error was then used to phase-lock the sensing laser acting on its current. The offset-lock of the two beatnotes is preferable than the use of independent optical cavities, because it ensures a tight phase-coherence between the reference and sensing lasers, which mitigates the impact of self-delayed lasers noise on the QKD interference pattern. This is possible because the self-delayed noise of the sensing laser is detected alongside with the optical fiber length variations and equally cancelled by the stabilization loop. As long as this noise is common with the reference laser, it is rejected from the QKD interference as well. An opposite mechanism would take place using independent lasers, in which case the self-delayed noise of the sensing laser would be written onto the QKD interference. A tight phase relation between the two lasers could be maintained even without using a frequency comb, relying on fast electro-optic modulators and sideband-locking [52].

Phase lock of the slave diode lasers

About 20 µW of the reference laser power was launched in the service fiber towards Alice and Bob terminals. Here, commercial diode lasers with an optical power <10 mW were phase-locked to it. To this purpose, we detected the beatnote between incoming and local light on a fast photodiode and compared it to a stable radio-frequency oscillator on a mixer in a quadrature condition. The phase error signal

was processed by a proportional-integrative-derivative controller acting on the laser current. The phase-locked-loop bandwidth of 1 MHz results from a combination of the frequency vs current response of the diode and the current driver's bandwidth.
The local oscillator for the phase-locked loop in Alice (Bardonecchia) was referenced to a 10 MHz signal disseminated with a White-Rabbit Precise Time Protocol over the service fiber, with short-term frequency stability of 1×10^{-11} [45,46]. In Bob (Santhià), where this service was not activated, we used a Rubidium oscillator with short term stability of 1×10^{-12}.

Cancellation of the fiber phase noise

The launched power of the sensing laser was about 1 mW into each arm of the interferometer. We stabilized the relative phase between the two return beams incoming in Charlie after travelling the path toward the remote terminals and back. To do so, we spilled out a portion of the sensing radiation before sending it to the remote terminals, and we detected the beatnote with the return signal on each arm. The resulting beatnotes at 40 MHz, the AOMs and AOMa frequencies, are down-scaled by a factor of 10 and phase-compared on a mixer in quadrature condition. The resulting error signal drives a proportional-integrative controller which adjusts the phase of both the sensing and QKD lasers by acting on the frequency of AOMa. The bandwidth of the phase-locked loop is limited to 50 kHz, which is large enough to fully compensate the acoustic noise introduced by the fiber and the residual self-delayed laser noise.

The normalised interference pattern

The pattern produced by the classical interference of the QKD lasers in Charlie is modelled as $I = 2I_0(1 + \cos\varphi)$ where I_0 is the lasers' intensity, assumed equal, and φ their phase difference. In the experiment, we equalised the intensities of the two beams and aligned their polarization to maximise the contrast. We then considered the normalised interference pattern $\bar{I} = I/4I_0 = \cos^2(\varphi/2)$, which can be regarded as the classical counterpart of a single photon interference. Operating the interferometer in a condition where $\varphi = 0$ or $\varphi = \pi$ corresponds to the case where all photons would be routed to one or the other port of the beamsplitter, i.e. operation in a dark port configuration. On the contrary, when the interferometer operates at $\varphi = \pi/2$ or $\varphi = 3\pi/2$, the probability of being detected on one or the other port are equal. In this condition, the phase fluctuations are directly mapped into intensity fluctuations, as in Fig. 3b. In our experiment, the residual phase fluctuations and its deviation are calculated from $\bar{I}$ inverting the related equation.

Statistical methods

The variance of the phase σ^2_φ, or its corresponding deviation σ_φ at a given measurement time t_a can be directly calculated from time domain data, or as the integral of the power spectrum, which in turns is calculated from instantaneous phase data. In our experiment, we adopted both methods. First, we computed the Welch periodogram of the phase $S_\varphi(f)$, as retrieved from the interference pattern, and integrated it between the Fourier frequencies $f = 1/t_\mathrm{a}$ and $f = f_\mathrm{s}/2$, where f_s is the sampling rate:

$$\sigma^2_\varphi = \int_{1/t_\mathrm{a}}^{f_\mathrm{s}/2} S_\varphi(f)\, df \tag{1}$$

We note that f_s must be at least twice as large as the noise bandwidth of the observed pattern to fulfil the Nyquist-Shannon sampling theorem [53]. In addition, we evaluated the phase variance over the time t_a by dividing the data set, composed of N phase samples φ_j and with total duration $T = N/f_\mathrm{s}$, in subsets of n points, where $n \approx N t_\mathrm{a}/T$. We then computed the standard deviation of each subset and averaged over the number of subsets $i \approx N/n$:

$$\sigma^2_\varphi = \langle \frac{1}{n-1} \Sigma^n_{j=0} (\varphi_j - \bar{\varphi})^2 \rangle_i \tag{2}$$

where $\bar{\varphi}$ is the average phase over each subset. We verified that both methods lead to the same result.
The obtained parameter is used to evaluate the QBER. When the interferometer is in the $\varphi \approx 0$ condition and all the counts are expected to be on a single detector, the QBER represents the probability of having clicks on the complementary one. The contribution to the QBER from decoherence is hence calculated from the phase noise of the system according to the relation

$$e = \int \left(1 - \cos^2(\varphi/2)\right) P(\varphi)\, d\varphi = \int \sin^2(\varphi/2) P(\varphi)\, d\varphi \tag{3}$$

As long as $\varphi \approx 0$, which is the only interesting case in practice, it can be seen that Eq. 3 is simplified to $e = \sigma_\varphi^2/4$, where σ_φ^2 is calculated from Eqs. 1 or 2. In Fig. 4 and throughout the text, we use this relation to evaluate the QBER.

Single photon detectors

We employed a commercial fiber-coupled InGaAs/InP avalanche detector (Id Quantique ID230). The detector mounts a Stirling cooler that enables to cool down to −90 °C, reducing the dark counts related to the detection process to a negligible level. It operates in free-running mode, enabling asynchronous photon detection with 150 ps timing resolution, in a spectral bandwidth ranging from 900 nm to 1700 nm. The quantum efficiency is variable up to 25% and its dead time can be adjusted from 2 µs to 100 µs.

Optical Filtering

Our technique is based on the transmission in the same fiber of two separate signals, the QKD lasers and the sensing laser, both in the C-band. Besides the issues related to nonlinear effects which generate background photons in the QKD lasers band, a key aspect is the efficient separation of the two signals in Charlie, to avoid that photons outside the QKD laser band reach the detector. This is primarily obtained with two cascaded 100 GHz-DWDM filters, each featuring 60 dB rejection at an offset of 1.5 nm from the central wavelength. However, the performances of standard telecom devices drop beyond 1300 nm, allowing a non-negligible power from the amplified spontaneous emission of the sensing laser, which extends to a wavelength of 1200 nm, to impinge the detectors. This was suppressed by placing a pair of additional free-space filters in front of the detectors, with nominal 50 dB rejection over the visible and near-IR band. Their 10 nm bandwidth, combined with the stronger selectivity of DWDM filters, ensured efficient filtering of the quantum photons. The overall losses of cascaded filtering stages amount to 2 dB, which is the result of the 84% transmissivity of the free-space filters and the coupling losses in the fiber/air interfaces.

References

[1] Bennett, C. H. & Brassard, G. Quantum cryptography: public key distribution and coin tossing. Theor. Comput. Sci. **560,** 7–11 (2014).

[2] Scarani, V. et al. The security of practical quantum key distribution. Rev. Mod. Phys. **81,** 1301 (2009).

[3] Kwong Lo, H., Curty, M. & Tamaki, K. Secure quantum key distribution. Nature Photonics **8,** 595-604 (2014).

[4] Dai, H. et al. Towards satellite-based quantum-secure time transfer, Nature Physics **16,** 848-852 (2020).

[5] Liao, S-K., Cai, W-Q., Pan, J-W. Satellite-to-ground quantum key distribution, Nature **549,** 43-47 (2017)

[6] Shimizu K., et al. Performance of long-distance quantum key distribution over 90-km optical links installed in a field environment of Tokyo metropolitan area. J. Lightwave Technol. **32,**, 141-51 (2014).

[7] Bacco, D. et al. Field trial of a three-state quantum key distribution scheme in the Florence metropolitan area. EPJ Quantum Technol.**6,** 5 (2019).

[8] Wengerowsky, S. et al. Entanglement distribution over a 96-km-long submarine optical fiber. PNAS **116,** 6684-6688 (2016).

[9] Mao, Y. et al. Integrating quantum key distribution with classical communications in backbone fiber network. Opt. Expr. **5,** 6010 (2018).

[10] Tanaka, A. et al. Ultra fast quantum key distribution over a 97 km installed telecom fiber with wavelength division multiplexing clock synchronization. Opt. Expr. **16,** 11354-11360 (2008).

[11] Choi, I. et al. Field trial of a quantum secured 10 Gb/s DWDM transmission system over a single installed fiber. Opt. Expr **22,** 23121-23128 (2014).

[12] Dixon, A. R. et al. Quantum key distribution with hacking countermeasures and long term field trial, Sci. Rep. **7,** 7583 (2017).

[13] Peev, M. et al. The SECOQC quantum key distribution network in Vienna, New J. Phys. **11,** 075001 (2009).

[14] Sasaki, M. et al. Field test of quantum key distribution in the Tokyo QKD Network. Opt. Expr. **19,** 10387 (2011).

[15] Dynes, J. F. et al. Cambridge quantum network. npj Quantum Inf. **5,** 101 (2019).

[16] Xu, F., Ma, X., Zhang, Q., Lo, H-K. & Pan, J-W. Secure quantum key distribution with realistic devices. Rev. Mod. Phys. **92,** 025002 (2020)

[17] Briegel, H. J., Dür, W., Cirac, J. I., & Zoller, P. Quantum Repeaters: The Role of Imperfect Local Operations in Quantum Communication, Phys. Rev. Lett. **81,** 5932 (1998).

[18] Sangouard, N., Simon, C., De Riedmatten, H., & Gisin, N. Quantum repeaters based on atomic ensembles and linear optics, Rev. Mod. Phys. **83,** 33 (2011).

[19] Lucamarini, M., Yuan, Z. L., Dynes, J. F., Shields, A. J. Overcoming the rate-distance limit of quantum key distribution without quantum repeaters. Nature **557,** 400-403 (2018).

[20] Ma, X. Zeng, P., & Zhou, H. Phase-Matching Quantum Key Distribution. Phys. Rev. X **8,** 031043 (2018).

[21] Wang, X-B., Yu, Z-W. & Hu, X-L. Twin-field quantum key distribution with large misalignment error. Phys. Rev. A **98,** 062323 (2018).

[22] Lin J. & Lutkenhaus, N. Simple security analysis of phase-matching measurement-device-independent quantum key distribution. Phys. Rev. A **98,** 042332 (2018);

[23] Curty, M., Azuma, K. & Lo, H.-K. Simple security proof of twin-field type quantum key distribution protocol. npj Quantum Inf. **5,** 64 (2019)

[24] Cui, C. et al., Twin-Field Quantum Key Distribution without Phase Postselection. Phys. Rev. Applied **11,** 034053 (2019).

[25] Yu, Z-W., Hu, X-L., Jiang, C., Xu, H. & Wang, X-B. Sending-or-not-sending twin-field quantum key distribution in practice. Sci. Rep. **9,** 3080 (2019).

[26] Yin, H-L. & Chen, Z-B. Finite-key analysis for twin-field quantum key distribution with composable security, Sci Rep. **9,** 17113 (2019).

[27] Lorenzo, G. C. et al., Tight finite-key security for twin-field quantum key distribution, arXiv:1910.11407 (2019)

[28] Xu, H., Yu, Z-W., Jiang, C., Hu, X-L. & Wang, X-B. Sending-or-not-sending twin-field quantum key distribution: Breaking the direct transmission key rate. Phys. Rev. A **101,** 042330 (2020).

[29] Wang, S. et al. Beating the Fundamental Rate-Distance Limit in a Proof-of-Principle Quantum Key Distribution System. Phys. Rev. X **9**, 021046 (2019)

[30] Minder, M. et al. Experimental quantum key distribution beyond the repeaterless secret key capacity. Nature Photon. **13**, 334-338 (2019)

[31] X. Zhong, Hu, J., Curty, M., Qian, L. & Lo, H-K. Proof-of-Principle Experimental Demonstration of Twin-Field Type Quantum Key Distribution. Phys. Rev. Lett. **123,** 100506 (2019)

[32] Chen, J-P. et al. Sending-or-Not-Sending with Independent Lasers: Secure Twin-Field Quantum Key Distribution over 509 km. Phys. Rev. Lett. **124,** 070501 (2020).

[33] Fang, X-T., et al. Implementation of quantum key distribution surpassing the linear rate-transmittance bound. Nature Photon **14**, 422-425 (2020).

[34] Clivati, C. et al. Optical frequency transfer over submarine fiber links. Optica **5**, 893 (2018).

[35] Clivati, C. et al. Common-clock very long baseline interferometry using a coherent optical fiber link. Optica **7,** 1031-1037 (2020)

[36] Grotti, J. et al. Geodesy and metrology with a transportable optical clock. Nature Physics **14**, 437-441 (2018).

[37] Lisdat, C. et al. A clock network for geodesy and fundamental science. Nat.Comm. **7**, 12443 (2016).

[38] Delva, P. et al. Test of Special Relativity Using a Fiber Network of Optical Clocks, Phys. Rev. Lett. **118,** 221102 (2017).

[39] Guena, J. First international comparison of fountain primary frequency standards via a long distance optical fiber link. Metrologia **54,** 348 (2017).

[40] Yamaguchi, A. et al. Direct comparison of distant optical lattice clocks at the 10^{-16} uncertainty. Appl. Phys. Expr. **4,** 082203 (2011).

[41] Boulder Atomic Clock Optical Network (BACON) Collaboration, Frequency ratio measurements with 18-digit accuracy using a network of optical clocks, arXiv:2005.14694.

[42] Williams, P. A. M., Swann, W. C. & Newbury, N. R. High-stability transfer of an optical frequency over long fiber-optic links. Jour. Opt. Soc. Am. B **25**, 1284 (2008).

[43] Clivati, C. et al. Planar-waveguide external cavity laser stabilization for an optical link with 10(-19) frequency stability. IEEE Trans. Ultrason. Ferroelectr. Freq. Control. **58**, 2582 (2011)

[44] Telle, H. R., Lipphardt, B. & Stenger, J. Kerr-lens, mode-locked lasers as transfer oscillators for optical frequency measurements. Appl. Phys. B **74**, 1:1-6 (2002)

[45] Serrano, J. et al. The White Rabbit Project, presented at the Int. Conf. Accelerator and Large Experimental Physics Control Systems (ICALEPCS), Kobe, Japan, 2009.

[46] Dierikx, E. F. et al. White Rabbit Precision Time Protocol on Long-Distance Fiber Links. IEEE Trans. Ultrason. Ferroel. Freq. Contr. **63**, 945 (2016).

[47] Alnis, J. et al. Ultralow noise miniature external cavity semiconductor laser. Phys. Rev. A **84**, 011804 (2011).

[48] Liang, W. et al. Ultralow noise miniature external cavity semiconductor laser. Nature Comm. **6**, 7371 (2015).

[49] Gobby, C., Yuan, Z. L., & Shields, A. J. Quantum key distribution over 122 km of standard telecom fiber. Appl. Phys. Lett. **84**, 3762 (2004).

[50] Liu, Y. et al. Experimental Twin-Field Quantum Key Distribution through Sending or Not Sending. Phys. Rev. Lett. **123**, 100505 (2019).

[51] Clivati, C. et al. A Large Area fiber Optic Gyroscope on multiplexed fiber network. Opt. Lett. **38**, 1092 (2014).

[52] Santagata, R. et al. High-precision methanol spectroscopy with a widely tunable SI-traceable frequency-comb-based mid-infrared QCL. Optica **6,** 411-423 (2019).

[53] Shannon, C. E. Communication in the presence of noise. Proc. Inst. Radio Engineers. **37,** 10-21 (1949).